Mechanical Reinforcement of Nanoparticle Thin Films Using Atomic Layer Deposition

Majemite I. Dafinone,[†] Gang Feng,[‡] Teresa Brugarolas,[†] Kwadwo E. Tettey,[†] and Daeyeon Lee[†,*]

[†]Department of Chemical and Biomolecular Engineering, University of Pennsylvania, Philadelphia, Pennsylvania 19104, United States, and [‡]Department of Mechanical Engineering, Villanova University, Villanova, Pennsylvania 19085, United States

ABSTRACT Thin films composed of nanoparticles exhibit synergistic properties, making them useful for numerous advanced applications. Nanoparticle thin films (NTFs), however, have a very low resistance to mechanical loading and abrasion, presenting a major bottleneck to their widespread use and commercialization. High-temperature sintering has been shown to improve the mechanical durability of NTFs on inorganic substrates; however, these high-temperature processes are not amenable to organic substrates. In this study, we demonstrate that the mechanical durability of TiO_2/SiO_2 nanoparticle layer-by-layer (LbL) films on glass and polycarbonate substrates can be drastically improved using atomic layer deposition (ALD) at a relatively low temperature. The structure and physical properties of ALD-treated TiO_2/SiO_2 nanoparticle LbL films are studied using spectroscopic ellipsometry, UV–vis spectroscopy, contact angle measurements, and nanoindentation. The composition of TiO_2/SiO_2 LbL films as a function of ALD-cycle number is determined through solution ellipsometry, enabling the determination of the characteristic pore size of nanoparticle thin films. Mechanical durability is also investigated by abrasion tests, showing that the robustness of ALD-treated nanoparticle films is comparable to that of thermally calcined films. More importantly, ALD-treated nanoparticle films retain the original functionality of the TiO_2/SiO_2 LbL films, such as superhydrophilicity and antireflection properties, demonstrating the utility of ALD as a reinforcement method for nanoparticle thin films.

KEYWORDS: atomic layer deposition · nanoparticle thin films · mechanical durability · layer-by-layer assembly · nanoindentation

Thin films are one of the most important structures that will enable the utilization of nanomaterial-based products for a variety of advanced applications including energy conversion and storage, electronics, optics, and biomedical applications.[1,2] The assembly of multiple nanomaterials into a thin film enables the generation of multifunctional structures with synergistic properties. While the possibilities for fabricating multifunctional thin films are endless, one of the major bottlenecks that prevents the widespread use of nanoparticle thin films (NTFs), we believe, is their poor mechanical reliability and durability.[3] Without mechanical reinforcement, these NTFs tend to fracture and abrade under small loads, making them unsuitable for commercial and industrial applications.

Thermal treatment of nanoparticle thin films at high temperatures (>500 °C), also known as calcination, improves their mechanical properties by sintering the nanoparticles together without significantly altering the morphology of the NTFs. However, calcination is not amenable for commercially important polymeric substrates, such as polycarbonate, and for NTFs that contain organic materials.[4] In addition, calcination may be adversely affected by the presence or, in some instances, by the absence of a chemical species in the substrate. For instance, the presence of sodium ions in a glass substrate has been shown to reduce the elastic modulus and hardness of an NTF upon calcination.[5] In contrast, another study found that the presence of sodium ions is essential for improving the adhesion of silica NTFs on glass substrates.[6]

Other thin film mechanical reinforcement methods that can be employed at relatively low temperatures (<200 °C) have been developed and investigated. These include the sorption and cross-linking of a polymerizable sol–gel precursor[7] and the chemical vapor deposition of inorganic precursors into particle assemblies.[8] These approaches, in general, have been shown to be suitable for assemblies involving colloidal particles that are larger than several hundred nanometers in size. The modification of nanoparticle thin films (composed of sub-100 nm nanoparticles) using these methods, however, could lead to undesirable changes in the film morphology such as the clogging of the pores due to capillary condensation.[9,10] It is also difficult to precisely control chemical vapor deposition and sorption processes, which may result in NTFs undergoing drastic changes in structure and functionality.[8]

More recently, hydrothermal calcination was shown to be effective in reinforcing

* Address correspondence to daeyeon@seas.upenn.edu.

Received for review March 28, 2011 and accepted May 10, 2011.

Published online May 10, 2011
10.1021/nn201167j

silica nanoparticle-containing thin films on polymer substrates.[6] This process can be used at a relatively low temperature of 121 °C, making it suitable for a variety of substrates including polymers. However, the process significantly alters the NTF morphology through a dissolution and redeposition mechanism. This morphology change could adversely affect the functionality of NTFs. For instance, silica nanoparticle thin films lose their superhydrophilicity upon hydrothermal calcination.[6]

In this study, we explore atomic layer deposition (ALD) as a method to reinforce nanoparticle thin films on inorganic and organic substrates. Atomic layer deposition is a self-limiting gas-phase nanofabrication method for growing atomic scale thin films of metal oxides and metals.[11] Unlike chemical vapor deposition (CVD), the gas precursors are pulsed sequentially and strictly separated from each other in the gas phase by a purge step, preventing gas-phase reactions and allowing the use of highly reactive precursors. This procedure results in the formation of films at low temperatures and provides the ability to precisely control the thickness of the desired layer.[12] ALD can be performed at a wide range of temperatures, from room temperature to 400 °C, making it an attractive method for modifying NTFs on polymer substrates.[11] A previous report demonstrates a simplified version of ALD, which uses tetramethoxysilane and ammonia vapor, which can be used to grow multiple silica layers.[13] These layers increase the stiffness of colloidal crystals made of ~300 nm particles. Other reports also demonstrate that the deposition of ultrathin Al_2O_3 by ALD on Li ion battery electrodes improves their capacity retention, cycling stability, and mechanical properties.[14−17]

The objective of this study is to investigate how ALD modifies the mechanical durability as well as the wetting and optical properties of all-nanoparticle thin films on both inorganic and organic substrates. In addition, we characterize the structural changes of nanoparticle thin films upon ALD treatment, which allows us to estimate the pore size of nanoparticle thin films. The NTFs used in this study are prepared by layer-by-layer assembly (LbL). This versatile method enables the preparation of uniform and conformal films over a large area.[3,18] LbL assembly of oppositely charged nanoparticles has been used to fabricate multifunctional NTFs; for example, a previous study has demonstrated that the sequential deposition of cationic TiO_2 and anionic SiO_2 nanoparticles leads to the generation of all-nanoparticle thin films with antireflection and antifogging properties.[19] We investigate the effect of ALD on the mechanical properties of TiO_2/SiO_2 nanoparticle LbL films by nanoindentation and an abrasion test. We also characterize other physical properties of ALD-treated NTFs using scanning electron microscopy, contact angle measurement, ellipsometry, and UV−vis spectroscopy.

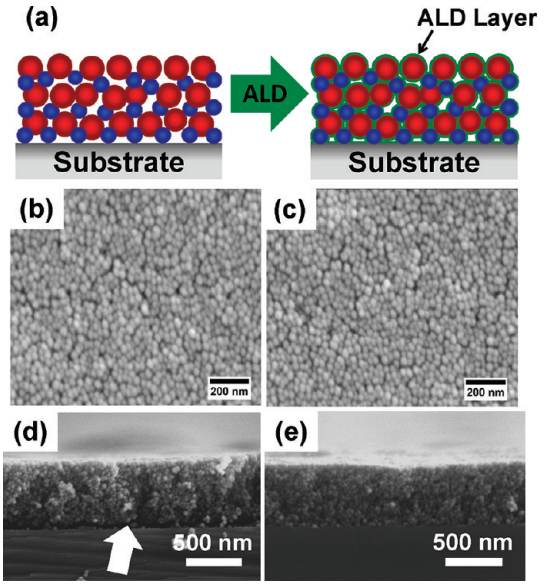

Figure 1. (a) Schematic illustration showing TiO_2/SiO_2 LbL films before (left) and after atomic layer deposition (right). Frontal-SEM images of 5-bilayer TiO_2/SiO_2 LbL films on glass (b) before and (c) after 10 Al_2O_3 ALD cycles. Cross-sectional SEM images of 25-bilayer TiO_2/SiO_2 LbL films on Si wafers (d) before and (e) after 10 Al_2O_3 ALD cycles. The white arrow in (d) indicates the delamination of the LbL film from the Si substrate (delamination in the as-assembled film is observed through the entire width of the SEM image).[28] Magnified images of the film/substrate interface are provided in Supporting Information (Figure S1)).

RESULTS AND DISCUSSION

Effect of Atomic Layer Deposition on the Structure of Layer-by-Layer Assembled Nanoparticle Thin Films. Atomic layer deposition is used to deposit conformal coatings of Al_2O_3 around nanoparticles in porous TiO_2/SiO_2 layer-by-layer thin films at 150 °C as illustrated in Figure 1a. ALD is a widely used method to generate conformal thin films over complex, porous structures.[20−22] To retain the superhydrophilicity of as-assembled TiO_2/SiO_2 nanoparticle LbL films, it is critical to maintain the network of interstitial void volume without blocking the pores.[19] Al_2O_3 ALD is chosen as the oxide coating because it is a well-defined ALD system[23] with very efficient surface reactions and is also known to adhere to various substrates.[24] Also, Al_2O_3 ALD has been shown to form conformal coatings around nanoparticles.[25−27]

Frontal-view scanning electron microscopy (SEM) (Figure 1b, c) of TiO_2/SiO_2 nanoparticle LbL films on glass before and after 10 cycles of Al_2O_3 ALD shows that the surface morphology of the LbL films is not drastically affected by the ALD process. The similarity in the SEM images is likely due to the thickness (~1 nm in total, 1.1 Å per cycle[23]) of the Al_2O_3 ALD layer being insignificant compared to the size (~22 nm) of silica nanoparticles (outermost layer) used in this study. Cross-sectional SEM images (Figure 1d, e) of 25-bilayer TiO_2/SiO_2 nanoparticle LbL films on Si wafers before and after 10 cycles of Al_2O_3 ALD also confirm that the

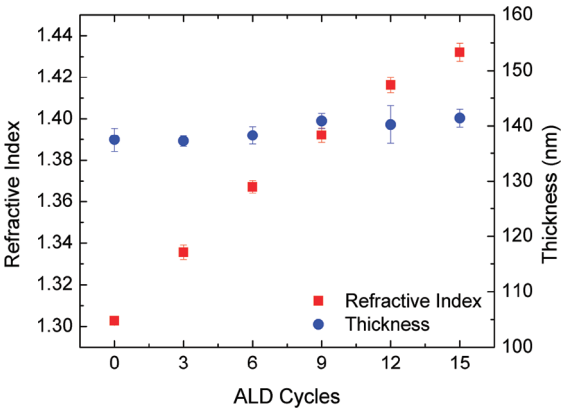

Figure 2. Film thickness and refractive index of 5-bilayer TiO_2/SiO_2 nanoparticle LbL films on glass as a function of the number of Al_2O_3 ALD cycles, determined by spectroscopic ellipsometry.

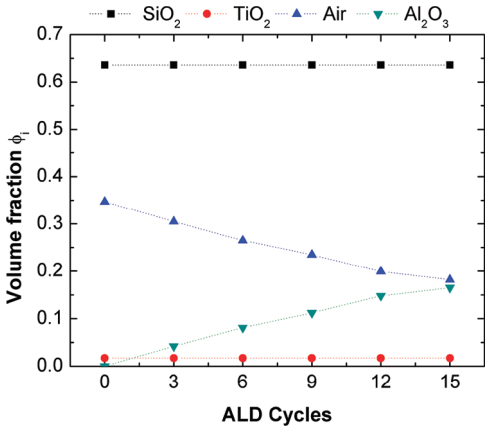

Figure 3. Volume fraction (ϕ_i) of each component (i) in TiO_2/SiO_2 5-bilayer LbL films on Si wafers with increasing ALD cycles determined using solution ellipsometry.

film thickness does not change upon ALD modification. However, it is interesting to note that during the preparation of the cross-section samples, the as-assembled TiO_2/SiO_2 LbL film delaminated from the substrate (white arrow in Figure 1d), whereas the ALD-treated nanoparticle film remained intact. This result is an indication that ALD improves the adhesion of TiO_2/SiO_2 nanoparticle films onto the substrates.

The thickness and refractive index of nanoparticle thin films treated with an increasing number of ALD cycles are determined using spectroscopic ellipsometry. Figure 2 reveals a pronounced increase in the refractive index of TiO_2/SiO_2 nanoparticle LbL films, which implies that successful ALD treatment was achieved; that is, Al_2O_3 coats around nanoparticles and reduces the void volume within the film.[29] In contrast, the change in film thickness due to the ALD treatment is negligible, and this result is consistent with the SEM images seen in Figure 1d, e.

A recently developed method based on solution ellipsometry enables the determination of thin film porosity and composition through the measurement of the effective refractive index of nanoporous films in air and in water.[19,30,31] We use this method to determine the composition of ALD-treated TiO_2/SiO_2 nanoparticle LbL films as a function of the number of ALD cycles. To use this method, the refractive indices of each component need to be determined. We obtain these values by generating single-component nanoparticle thin films of either TiO_2 or SiO_2 nanoparticles (see Supporting Information for details).[19] Through this method, the refractive indices of TiO_2 and SiO_2 nanoparticles are determined to be 2.30 and 1.44, respectively. The refractive index of Al_2O_3 at 633 nm is determined to be 1.73 from the spectroscopic ellipsometry of an Al_2O_3 ALD film (100 cycles) deposited on a Si wafer. This value is consistent with the previously reported values of refractive index for ALD-deposited Al_2O_3, which lie between 1.5 and 1.7.[23,32,33]

The effect of increasing ALD cycles on the porosity and composition of each component in TiO_2/SiO_2 nanoparticle LbL films on Si wafers is plotted in Figure 3. As the deposition proceeds, the volume fraction of air (*i.e.*, porosity) decreases, while that of deposited Al_2O_3 increases. These results agree with the idea that although ALD does not drastically change the thickness of the entire film as illustrated in Figure 1a, it leads to the generation of conformal Al_2O_3 layers around nanoparticles, which reduces the porosity of the films.

Characterization of the porosity of TiO_2/SiO_2 nanoparticle LbL films as a function of ALD cycles provides a unique opportunity to determine the pore size of TiO_2/SiO_2 LbL films. It has been challenging to directly determine the pore size of these nanoparticle thin films using traditional methods such as BET measurements because of the limited volume of thin films that are typically generated. We develop a simple model that relates the change in porosity to the characteristic pore size (d_p) of TiO_2/SiO_2 LbL films (for details see Supporting Information). These nanoparticle LbL films have a tortuous network of pores; thus, the pore morphology is not easily defined. To obtain a reasonable range for the characteristic pore size, we estimate d_p for two-dimensional and three-dimensional pores, of which pore volume scales as d_p^2 and d_p^3, respectively.

The simple model that relates the porosity to the number of ALD cycles (x) (Figure 4) can be expressed as

$$P(x) = \frac{P_0(d_p - 2xt)^n}{d_p^n} \quad (1)$$

where $n = 2$ and 3 for 2-D (*e.g.*, cylindrical) and 3-D (*e.g.*, spherical) pores, respectively. P, d_p, x, and t represent the porosity, initial characteristic pore size, number of ALD cycles, and thickness of each ALD layer, respectively. By fitting eq 1 to the change in the porosity (Figure 3) as a function of the number of ALD cycles, the average initial pore size of the as-assembled 7 nm TiO_2/22 nm SiO_2 LbL films is determined as 11.3 nm for 2-D pores and 16.3 nm for 3-D pores. This result is

consistent with previous studies, which show that the pore size in various random aggregates of nanoparticles is similar to or smaller than the size of the nanoparticles.[34−38]

On the basis of the estimated pore size, we can verify that the precursor exposure time employed during ALD is suitable to treat nanoporous TiO_2/SiO_2 LbL films uniformly. ALD on these nanoparticle thin films is controlled by the Knudsen diffusion of trimethylaluminum (TMA) and water within the pores since the mean free paths of these molecules are much greater than the size of the pores (*i.e.*, Knudsen number >1).[21,39,40] The minimum exposure time required for uniform surface coverage can be calculated (for details see Supporting Information) by determining the diffusion coefficient of the precursors.[40,41] The Knudsen diffusivity of TMA from kinetic theory is $\sim 10^{-8}$ m^2/s. The minimum exposure time required (τ) for nanoparticle thin films (thickness =150 nm) is estimated to be on the order of 10^{-3} s. This time is much smaller than the actual exposure time (~5 s) of TMA and water during ALD. We further extend our analysis to estimate τ for TMA as a function of ALD cycles because repeated ALD deposition will decrease the pore size and, in turn, increase τ (see Supporting Information for details).[42] This analysis shows that the employed ALD exposure time is much greater than the minimum exposure time needed even if the pores become smaller due to ALD treatment. Thus, we believe the ALD parameters used in this study are sufficient to uniformly treat our TiO_2/SiO_2 LbL thin films.

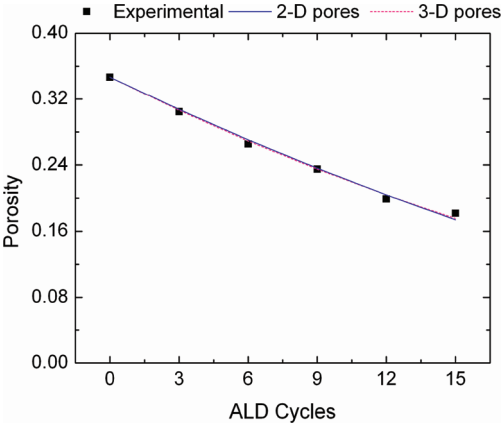

Figure 4. Determination of pore size of TiO_2/SiO_2 nanoparticle LbL films on Si wafers based on eq 1. Filled squares represent porosity obtained from solution ellipsometry. Solid blue line and dotted red line represent the fitting of eq 1 to the experimental results using 2-D and 3-D pore models, respectively.

Effect of Atomic Layer Deposition on the Superhydrophilicity of TiO_2/SiO_2 Nanoparticle Layer-by-Layer Films. TiO_2/SiO_2 nanoparticle LbL films are superhydrophilic; that is, water spreads on the surface with a contact angle of less than 5° within 0.5 s because of the presence of nanoscale interstitial pores.[19,43] The superhydrophilicity of the nanoparticle films results in antifogging properties, making them useful in numerous practical applications. It is important that TiO_2/SiO_2 LbL films retain this useful property after mechanical reinforcement. Therefore, the contact angle of water is measured on ALD-treated LbL films on top of glass and polycarbonate substrates.

The contact angle of water on TiO_2/SiO_2 films on glass is observed to increase with the number of ALD cycles, as seen in Figure 5a.[44] During Al_2O_3 ALD, it is likely that organic residues from the precursors, such as excess methyl groups, remain on the surface after deposition. Impurities in the films have been reported to be at the 0.1−1 atom % level.[12] To completely remove such organic residues, ALD-modified TiO_2/SiO_2 LbL films are treated with oxygen plasma. In all cases, superhydrophilicity (contact angle less than 5°) is restored in the films, and these films remain superhydrophilic even after 30 days.

The wetting behavior of TiO_2/SiO_2 nanoparticle LbL films deposited on polycarbonate substrates is also

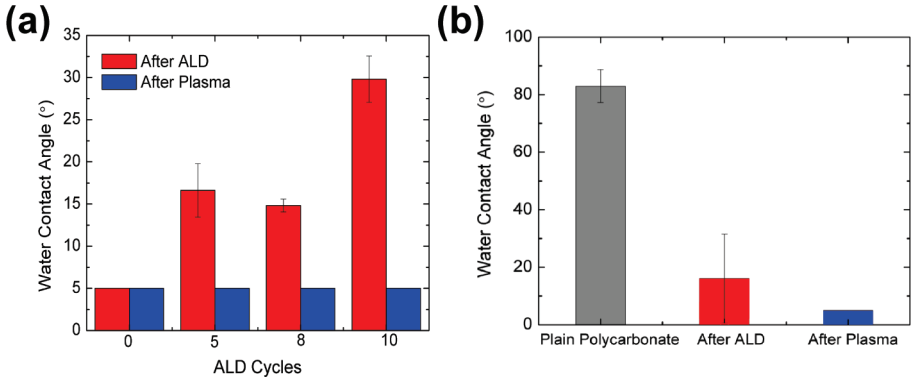

Figure 5. Water contact angle of TiO_2/SiO_2 LbL films with increasing ALD cycles on (a) glass and (b) polycarbonate substrates before and after plasma treatment. "After ALD" and "After Plasma" in (b) denote the water contact angle on ALD-treated SiO_2/TiO_2 LbL films atop Al_2O_3-primed polycarbonate before and after plasma treatment, respectively. Error bars are the standard deviation of at least three contact angle measurements. Contact angle of 5° denotes complete spreading, which makes it difficult to exactly determine the contact angle. The actual value of the contact angle in such cases is less than 5°.

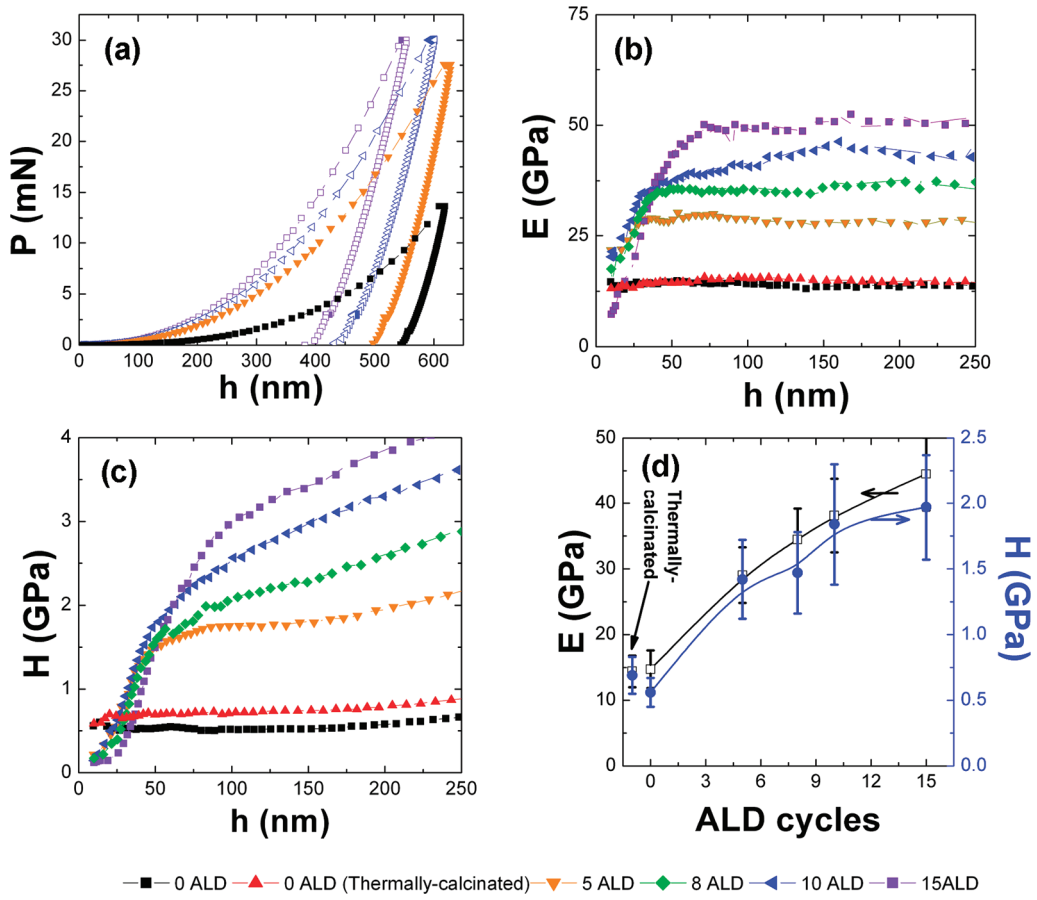

Figure 6. Nanoindentation results as a function of ALD cycles (from 0 to 15) for TiO_2/SiO_2 LbL films on Si wafers. (a) The indentation load (P) as a function of indentation depth (h) ($h = 0$ nm at the LbL film surface). (b) Modulus (E) and (c) hardness (H) as a function of h. (d) E (plateau values) and H as a function of the number of ALD cycles, where each point is the statistical average for the corresponding CSM results of 36 tests and in the region of $h = 9.5-10.5\%$ of the film thickness. Data in (b) are the results after correcting for the substrate effect.[51] Red triangles represent results obtained from thermally calcinated samples.

studied. Unmodified polycarbonate is inherently hydrophobic (Figure 5b). This hydrophobicity combined with the lack of electrostatic interactions between polycarbonate and charged nanoparticles causes nonuniform deposition of TiO_2/SiO_2 LbL films on unmodified polycarbonate.[45] Recent studies have shown that homogeneous oxide thin films can be formed on polymer surfaces using ALD.[23,46,47] We find that priming the polycarbonate substrates with Al_2O_3 ALD (100 cycles) coatings before LbL assembly significantly improves the uniformity of TiO_2/SiO_2 films. Zeta potential measurements show that the ALD-deposited Al_2O_3 layer has a positive surface potential of 20.6 ± 4 mV. Therefore, ALD-treated polycarbonate has a net positive surface charge, facilitating the uniform deposition of negatively charged SiO_2 nanoparticles and, subsequently, the alternate deposition of the two nanoparticles. ALD-treated SiO_2/TiO_2 LbL films on ALD-modified polycarbonate become highly hydrophilic, as shown in Figure 5b. Subsequent oxygen plasma treatment renders the surface superhydrophilic, demonstrating the importance of removing organic residues. As will be discussed in detail later, the pretreatment of polycarbonate with Al_2O_3 ALD is also critical in enhancing the mechanical durability of the nanoparticle thin films.

Effect of Atomic Layer Deposition on the Mechanical Properties of Layer-by-Layer Assembled Nanoparticle Thin Films. The effect of ALD on the small-scale mechanical properties of TiO_2/SiO_2 nanoparticle thin films is characterized using nanoindentation. Nanoindentation provides quantitative information on the applied force (P) and the corresponding indentation depth (h) for describing the mechanical behavior of thin films (Figure 6a).[48] A continuous stiffness measurement (CSM) technique is employed, which enables continuous measurement of the elastic contact stiffness (S)—and thus hardness (H) and modulus (E)—of ALD-treated TiO_2/SiO_2 LbL films by superimposing a small harmonic force on the quasi-static main load.[49]

On the basis of the CSM technique, we confirm that the modulus (E) and hardness (H) of TiO_2/SiO_2 LbL films on Si wafers increase drastically and systematically with increasing ALD cycles, as seen in Figure 6. We find that the modulus and the hardness, calculated on the basis of the conventional Oliver–Pharr method,

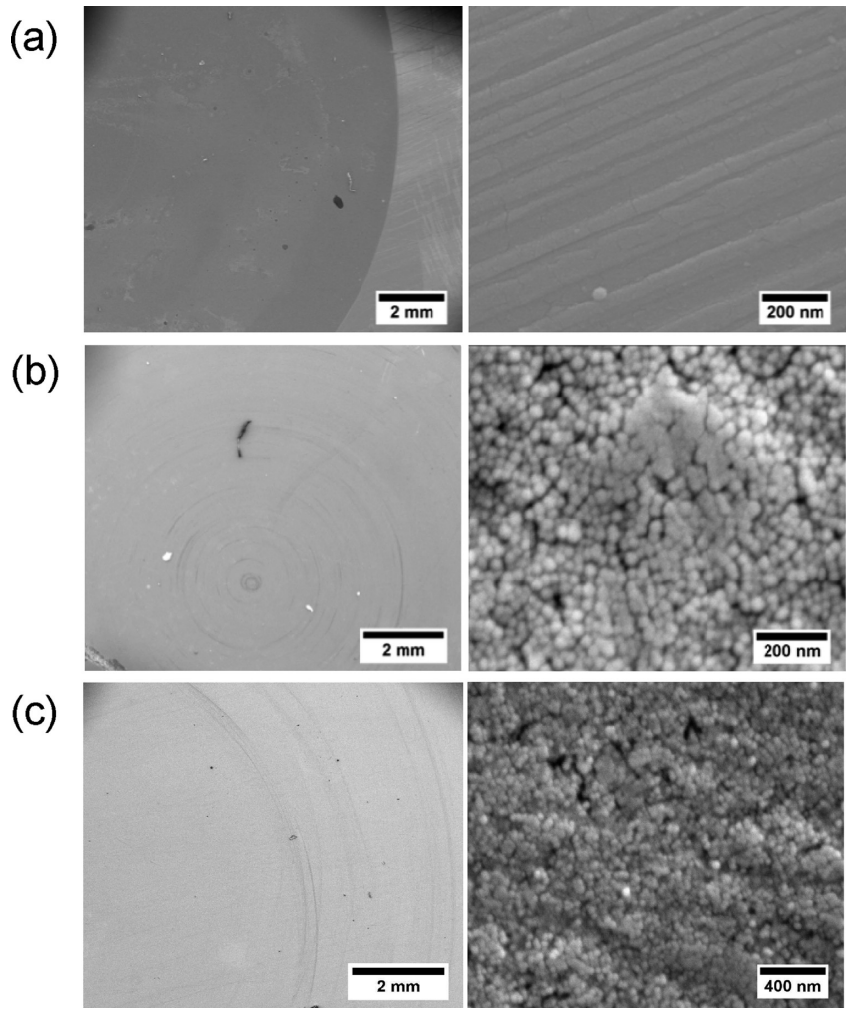

Figure 7. SEM micrographs of (a) 5-bilayer TiO_2/SiO_2 nanoparticle LbL films on glass; (b) 5-bilayer TiO_2/SiO_2 films treated with 10 Al_2O_3 ALD on glass; (c) 5-bilayer SiO_2/TiO_2 films treated with 8 Al_2O_3 ALD on polycarbonate primed with 100 Al_2O_3 ALD. Images in the left and right columns are taken at low and high magnification, respectively.

increase with the indentation depth *h* without a plateau region (Figure S3 and Figure 6c). This absence of plateau regions is likely due to the effect of the stiffer and harder Si substrate[49−51] (the hardness for 0 ALD TiO_2/SiO_2 LbL films shows plateau regions). We correct the modulus data for the substrate effect using a recently introduced method as shown in Figure 6b.[51] The substrate-effect-corrected modulus reaches a plateau for indentation depth (*h*) greater than 50 nm. In Figure 6c, the steep hardness increase in the region of $0 < h < 50$ nm is mainly due to the surface roughness. It is well-known that the hardness would be underestimated if *h* is comparable with the surface roughness (about 20 nm for the nanoparticle thin films[19]) due to the contribution of the incompact surface to the indented volume.[52] Figure 6d summarizes the increase in the modulus and hardness of ALD-treated films with the number of ALD cycles (the black and blue curves represent the modulus (*E*) and hardness (*H*), respectively). The first pair of data points, outside the curves, is the modulus and hardness of a thermally calcinated sample. Interestingly, the *E* and *H* of thermally calcinated nanoparticle thin films are inferior to those of ALD-treated samples (Figure 6d), illustrating the potential of ALD as a highly effective reinforcement approach for various nanoparticle thin films.

The macroscopic mechanical durability of ALD-treated nanoparticle thin films is tested under mechanical shear using an abrasion testing protocol. A normal stress of 30 kPa is applied on the films with a rotational shear of 150 rpm, which is similar to an ASTM method, ASTM D 1044, to test the durability of optical coatings (see Supporting Information for details).[6] After abrasion testing, the films are characterized using scanning electron microscopy as seen in Figure 7. As-assembled films, without ALD treatment, on glass are completely abraded and delaminated from the substrates (Figure 7a). Nanoparticle films on glass with 10 cycles of Al_2O_3 ALD show a small number of circular scratches visible at a low magnification (Figure 7b, left). On the basis of the high magnification SEM images, these scratches are revealed as regions with flattened nanoparticle layers

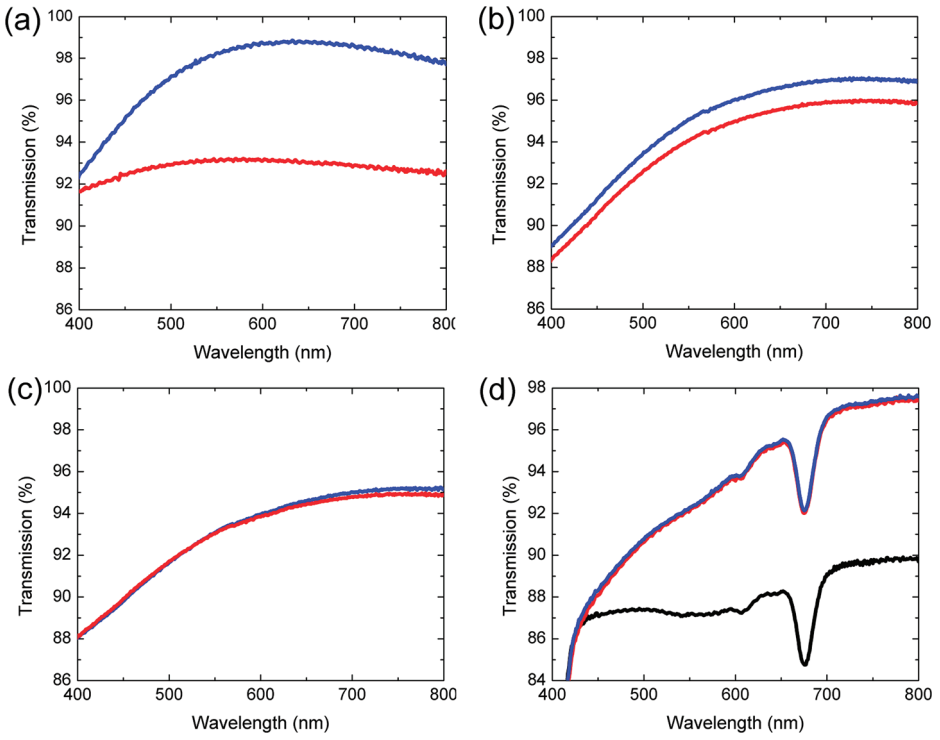

Figure 8. UV−vis spectra of 5-bilayer TiO_2/SiO_2 nanoparticle LbL films on glass treated with (a) 0, (b) 5, and (c) 10 Al_2O_3 ALD cycles. (d) 5-bilayer SiO_2/TiO_2 LbL films treated with 8-Al_2O_3 ALD cycles on ALD-primed polycarbonate (100 Al_2O_3 ALD cycles) before and after abrasion testing. Blue and red curves represent transmission spectra before and after 30 kPa abrasion testing, respectively. Black curve represents the spectrum of unmodified polycarbonate substrate used in this study.

(Figure 7b, right) showing good adhesion to the substrate rather than regions of film delamination. Similar flattening has previously been reported and is attributed to the deformation of nanoparticle films under the influence of frictional heating and tribochemical wear.[6] It can be inferred from these results that ALD improves adhesion between nanoparticle thin films and their substrate and uniformly modifies the entire nanoparticle thin films (*i.e.*, from top to bottom); otherwise, these nanoparticle thin films would undergo complete delamination during the abrasion test.

Abrasion testing is also performed on TiO_2/SiO_2 nanoparticle LbL films on polycarbonate. The ALD-treated TiO_2/SiO_2 LbL films on unmodified polycarbonate are completely delaminated during abrasion testing. LbL assembly on polycarbonate is challenging due to the weak interfacial adhesion between the inorganic nanoparticles and the polymer surface.[45] As described earlier, the priming of polycarbonate substrates with a ~10 nm Al_2O_3 ALD layer (100 Al_2O_3 ALD cycles) is critical for enhancing the uniformity of the deposited LbL films. More importantly, a subsequent ALD treatment of SiO_2/TiO_2 LbL films on ALD-primed polycarbonate drastically improves the abrasion resistance of the nanoparticle films, as seen in Figure 7c. The absence of the Al_2O_3 primer layer on polycarbonate results in relatively weak films even after ALD treatment. We believe the effectiveness of ALD treatment on the nanoparticle films is enhanced due to the improved adhesion of nanoparticles to the Al_2O_3 primer layer. Our results clearly indicate the importance of pretreating polycarbonate substrates with an Al_2O_3 primer layer.

The effect of abrasion testing on ALD-treated TiO_2/SiO_2 nanoparticle LbL films is also determined by optical characterization. As-assembled TiO_2/SiO_2 LbL films have antireflection properties and increase the peak transmission of glass to approximately 99%; thus, any mechanical damages to the film would compromise its optical property.[19] After the abrasion of as-assembled TiO_2/SiO_2 LbL films on glass, the nanoparticles are completely removed from the surface and the transmission in the visible range (400−700 nm) decreases substantially as shown in Figure 8a. Figure 8b, c shows that the peak transmission of the nanoparticle film-coated glass treated with 5 and 10 cycles of Al_2O_3 ALD is 98% and 95%, respectively. This reduction in the antireflection properties is attributed to the increased refractive index of the films upon ALD treatment. However, Figure 8b, c shows that the difference in transmission before and after abrasion decreases with an increasing number of ALD cycles, indicating an improvement in mechanical durability. These results demonstrate that there is a trade-off between antireflection property and mechanical durability for ALD-treated nanoparticle thin films on glass.

The effectiveness of ALD as a reinforcement method is clearly demonstrated when a polycarbonate substrate

is used. The presence of an ALD-treated SiO_2/TiO_2 LbL film on ALD-primed polycarbonate drastically reduces the reflection, as seen in Figure 8d. Unmodified polycarbonate has a peak transmission of 88% in the visible range,[53] whereas ALD-treated SiO_2/TiO_2 films improve the peak transmission to 98% due to the dramatic suppression of reflection. Abrasion testing on the treated surface has a negligible effect on the antireflection properties, illustrating the robustness of these films after ALD. Considering that these SiO_2/TiO_2 LbL films on polycarbonate cannot be mechanically reinforced using thermal calcination, the obtained results based on ALD are significant. Our results clearly demonstrate that ALD is a useful method to impart mechanical robustness to all-nanoparticle thin films on polycarbonate substrates without substantially compromising the useful superhydrophilic and antireflection properties.

CONCLUSION

In summary, we have demonstrated that atomic layer deposition is a versatile method for imparting mechanical durability to nanoparticle thin films on inorganic and organic substrates without drastically changing the structure and functional properties of the NTFs. In addition, by measuring the porosity as a function of ALD cycles using solution ellipsometry, we determine the characteristic pore size of TiO_2/SiO_2 nanoparticle LbL films. Our results based on the minimum exposure time (τ) analysis and the abrasion test strongly indicate that Al_2O_3 ALD uniformly coats TiO_2/SiO_2 nanoparticle LbL films from the substrate to the top surface. The ability to use low-temperature ALD to reinforce NTFs on polymers is essential, as polymers and plastics are widely used in various applications such as food packaging, flexible electronic devices, and biomedical devices.[46,54−56] In addition to mechanical reinforcement, ALD presents a unique opportunity to deposit various oxides and metals that could impart additional functionalities, such as catalytic and electrical properties,[57−60] to nanoparticle thin films, making these films more attractive for various advanced applications.[45,61]

METHODS

Materials. Anatase titanium dioxide nanoparticles, STS-100 (18 wt % TiO_2 suspension in water, average particle size of 7 nm, and specific surface area of 320 m^2/g), were generously provided by Ishihara Sangyo Kaisha, Ltd. (Japan). Silica nanoparticles, Ludox TM-40 (40 wt % SiO_2 suspension in water, average particle size of 22 nm, and specific surface area of 140 m^2/g), were purchased from Sigma-Aldrich (St. Louis, MO). The average size of nanoparticles is provided by the suppliers. Glass slides were purchased from Fisher. Polycarbonate sheets were purchased from Small Parts, Inc.

Layer-by-Layer Assembly. Seven nanometer TiO_2 and 22 nm SiO_2 nanoparticles are used for layer-by-layer assembly. Nanoparticles are diluted to 0.03 wt % in deionized (DI) water (18.2 MΩ-m, Barnstead Nanopure), and each suspension is adjusted to pH 3.0 with HCl. The exposure time of substrates in nanoparticle suspensions is 10 min. The three rinse steps in DI water are 2, 1, and 1 min long. Glass substrates are degreased by sonication in 1.0 M NaOH for 15 min. The substrates are then thoroughly rinsed with DI water and dried with compressed air. Layer-by-layer deposition is performed using a HMS series programmable slide stainer from Carl Zeiss, Inc.

Atomic Layer Deposition. Al_2O_3 layers are deposited at 150 °C on TiO_2/SiO_2 nanoparticle LbL films using a Savannah 200 atomic layer deposition system from Cambridge NanoTech Inc. Before deposition, samples are placed in the ALD chamber and heated to 150 °C. The temperature is maintained at 150 °C during the deposition.[62] For Al_2O_3 ALD, trimethylaluminum and water vapor are sequentially pulsed through the reaction chamber.[11] N_2 gas is used to purge the chamber after injecting each precursor. A monolayer is formed after each ALD growth cycle, and film growth occurs monolayer by monolayer until the desired thickness is obtained. The reaction sequence for Al_2O_3 deposition on plain polycarbonate before layer-by-layer assembly is (i) H_2O dose for 0.015 s; (ii) purge for 20 s; (iii) TMA dose for 0.015 s; and (iv) purge for 20 s.

For ALD on highly porous films, the precursors are pumped in between pulses, with the stop valve closed (exposure mode).[42] The Al_2O_3 ALD reaction sequence on LbL films is (i) close stop valve, which fills the reactor with nitrogen; (ii) H_2O dose for 0.015 s; (iii) wait time of 5 s to allow precursor gas to diffuse through the sample; (iv) open stop valve; (v) purge for 5 s; (vi) close stop valve; (vii) TMA dose for 0.015 s; (viii) wait time of 5 s; (ix) open stop valve; and (x) purge system for 5 s.

Characterization. Thickness and refractive indices of TiO_2/SiO_2 nanoparticle LbL films are determined using a spectroscopic ellipsometer, Alpha-SE, and the Complete EASE software package (J.A. Woollam). Refractive index values are obtained at the wavelength of 633 nm. The transmission spectra of samples in the 400−800 nm range are recorded by a Cary 5E UV−vis−NIR spectrophotometer (Varian, Inc.). Scanning electron microscopy is performed using an FEI 600 Quanta FEG ESEM at 5 kV. All samples are sputter-coated with Au/Pd prior to imaging and are mounted onto SEM stubs using double-sided carbon tape.

The mechanical properties are characterized by nanoindentation using a Nano Indenter G200 from Agilent Technologies Inc. with enhanced dynamic contact module (DCM II) and continuous stiffness measurement. A Berkovich indenter and the DCM II are used to perform indentations. The tip area function is calibrated using fused silica, and a constant modulus E is achieved in a depth range of 5−500 nm. Before performing any indentation, the indenter is stabilized to achieve a thermal drift rate less than 0.05 nm/s. For all indentations, constant strain rate (0.05 s^{-1}) loading is used. The CSM option allows the depth profiles of the mechanical properties to be tested, and the CSM harmonic displacement (amplitude) is set as 0.5 nm. For each sample, a 6 × 6 array is performed, and the result of each 6 × 6 array is then analyzed using Agilent Analyst software to determine the statistical results.

Surface zeta potential measurement of 100 ALD layers of Al_2O_3 is performed using a Delsa Nano C (Beckman Coulter). A flat surface cell in which the coated Si wafer forms the upper cell surface is used. To probe the charge state of the surface, standard latex particles (Beckman Coulter) are used. The velocity profile of the standard latex particles undergoing electrophoresis through the flat surface cell is fitted to the Mori and Okamoto equation.[63] From this fit, the zeta potential of the film is calculated using the Smoluchowski equation as $\zeta = (\mu \times \eta)/(\varepsilon_\gamma \times \varepsilon_o)$. In this equation, ζ represents the zeta potential (V), μ the electrophoretic mobility ($m^2/(V\ s)$), and η the viscosity of water (Pa·s); ε_o (F/m) and ε_r are the dielectric constants of vacuum and water, respectively.

Mechanical durability of the films is determined by applying a rotational shear stress to the films. This abrasion test is adopted from a standard cleaning cloth abrasion test described in ASTM D 1044, which uses a normal stress of approximately 28 kPa (see Supporting Information for details).

Acknowledgment. This work was supported primarily by an NSF CAREER Award (DMR-1055594) and partly by the PENN MRSEC DMR-0520020 and the PENN NSEC DMR-0425780. We thank Professors Russell Composto and Cherie Kagan (University of Pennsylvania) for the use of their UV−vis spectrophotometers, Professor Shu Yang and Dr. Raghuraman (University of Pennsylvania) for the use of the goniometer. We also thank Steve Szewczyk (University of Pennsylvania) for the use of the metal polisher, and Iulian Codreanu, Brett Goldsmith, and Kyle Keenan (University of Pennsylvania) for the use of the Wolf Nanofabrication facility and atomic layer deposition tool. F.G. acknowledges the support from Agilent Technologies and the Keystone Innovation Starter Kit (KISK) award from the Pennsylvania Department of Community and Economic Development. T.B. acknowledges the graduate fellowship from Fundación Caja Madrid.

Supporting Information Available: Additional information on the pore size model, the composition determination of ALD-treated nanoparticle thin films, the estimation of minimum ALD exposure time, uncorrected modulus data based on nanoindentation, and the experimental procedure for the abrasion test. This material is available free of charge *via* the Internet at http://pubs.acs.org.

REFERENCES AND NOTES

1. Jiang, C. Y.; Tsukruk, V. V. Freestanding Nanostructures *via* Layer-by-Layer Assembly. *Adv. Mater.* **2006**, *18*, 829–840.
2. Markutsya, S.; Jiang, C. Y.; Pikus, Y.; Tsukruk, V. V. Freely Suspended Layer-by-Layer Nanomembranes: Testing Micromechanical Properties. *Adv. Funct. Mater.* **2005**, *15*, 771–780.
3. Shimomura, H.; Gemici, Z.; Cohen, R. E.; Rubner, M. F. Layer-by-Layer-Assembled High-Performance Broadband Antireflection Coatings. *ACS Appl. Mater. Interfaces* **2010**, *2*, 813–820.
4. Latella, B. A.; Triani, G.; Zhang, Z.; Short, K. T.; Bartlett, J. R.; Ignat, M. Enhanced Adhesion of Atomic Layer Deposited Titania on Polycarbonate Substrates. *Thin Solid Films* **2007**, *515*, 3138–3145.
5. Yaghoubi, H.; Taghavinia, N.; Alamdari, E. K.; Volinsky, A. A. Nanomechanical Properties of TiO_2 Granular Thin Films. *ACS Appl. Mater. Interfaces* **2010**, *2*, 2629–2636.
6. Gemici, Z.; Shimomura, H.; Cohen, R. E.; Rubner, M. F. Hydrothermal Treatment of Nanoparticle Thin Films for Enhanced Mechanical Durability. *Langmuir* **2008**, *24*, 2168–2177.
7. Rouse, J. H.; MacNeill, B. A.; Ferguson, G. S. Sol-Gel Processing of Ordered Multilayers to Produce Composite Films of Controlled Thickness. *Chem. Mater.* **2000**, *12*, 2502–2507.
8. Miguez, H.; Chomski, E.; Garcia-Santamaria, F.; Ibisate, M.; John, S.; Lopez, C.; Meseguer, F.; Mondia, J. P.; Ozin, G. A.; Toader, O.; *et al.* Photonic Bandgap Engineering in Germanium Inverse Opals by Chemical Vapor Deposition. *Adv. Mater.* **2001**, *13*, 1634–1637.
9. Liang, X. H.; George, S. M.; Weimer, A. W. Synthesis of a Novel Porous Polymer/Ceramic Composite Material by Low-Temperature Atomic Layer Deposition. *Chem. Mater.* **2007**, *19*, 5388–5394.
10. Gemici, Z.; Schwachulla, P. I.; Williamson, E. H.; Rubner, M. F.; Cohen, R. E. Targeted Functionalization of Nanoparticle Thin Films *via* Capillary Condensation. *Nano Lett.* **2009**, *9*, 1064–1070.
11. George, S. M. Atomic Layer Deposition: An Overview. *Chem. Rev.* **2010**, *110*, 111–131.
12. Leskela, M.; Ritala, M. Atomic Layer Deposition Chemistry: Recent Developments and Future Challenges. *Angew. Chem., Int. Ed.* **2003**, *42*, 5548–5554.
13. Hatton, B.; Kitaev, V.; Perovic, D.; Ozin, G.; Aizenberg, J. Low-Temperature Synthesis of Nanoscale Silica Multilayers−Atomic Layer Deposition in a Test Tube. *J. Mater. Chem.* **2010**, *20*, 6009–6013.
14. Scott, I. D.; Jung, Y. S.; Cavanagh, A. S.; Yan, Y.; Dillon, A. C.; George, S. M.; Lee, S.-H. Ultrathin Coatings on Nano-$LiCoO_2$ for Li-Ion Vehicular Applications. *Nano Lett.* **2011**, *11*, 414–418.
15. Jung, Y. S.; Cavanagh, A. S.; Riley, L. A.; Kang, S. H.; Dillon, A. C.; Groner, M. D.; George, S. M.; Lee, S. H. Ultrathin Direct Atomic Layer Deposition on Composite Electrodes for Highly Durable and Safe Li-Ion Batteries. *Adv. Mater.* **2010**, *22*, 2172–2176.
16. Riley, L. A.; Cavanagh, A. S.; George, S. M.; Lee, S.-H.; Dillon, A. C. Improved Mechanical Integrity of ALD-Coated Composite Electrodes for Li-Ion Batteries. *Electrochem. Solid-State Lett.* **2011**, *14*, A29–A31.
17. Jung, Y. S.; Cavanagh, A. S.; Dillon, A. C.; Groner, M. D.; George, S. M.; Lee, S. H. Enhanced Stability of $LiCoO_2$ Cathodes in Lithium-Ion Batteries using Surface Modification by Atomic Layer Deposition. *J. Electrochem. Soc.* **2010**, *157*, A75–A81.
18. Podsiadlo, P.; Sui, L.; Elkasabi, Y.; Burgardt, P.; Lee, J.; Miryala, A.; Kusumaatmaja, W.; Carman, M. R.; Shtein, M.; Kieffer, J.; *et al.* Layer-by-Layer Assembled Films of Cellulose Nanowires with Antireflective Properties. *Langmuir* **2007**, *23*, 7901–7906.
19. Lee, D.; Rubner, M. F.; Cohen, R. E. All-Nanoparticle Thin Film Coatings. *Nano Lett.* **2006**, *6*, 2305–2312.
20. Cleveland, E. R.; Banerjee, P.; Perez, I.; Lee, S. B.; Rubloff, G. W. Profile Evolution for Conformal Atomic Layer Deposition over Nanotopography. *ACS Nano* **2010**, *4*, 4637–4644.
21. Elam, J. W.; Routkevitch, D.; Mardilovich, P. P.; George, S. M. Conformal Coating on Ultrahigh-Aspect-Ratio Nanopores of Anodic Alumina by Atomic Layer Deposition. *Chem. Mater.* **2003**, *15*, 3507–3517.
22. Lakomaa, E. L. Atomic Layer Epitaxy (ALE) on Porous Substrates. *Appl. Surf. Sci.* **1994**, *75*, 185–196.
23. Groner, M. D.; Fabreguette, F. H.; Elam, J. W.; George, S. M. Low-Temperature Al_2O_3 Atomic Layer Deposition. *Chem. Mater.* **2004**, *16*, 639–645.
24. Jur, J. S.; Spagnola, J. C.; Lee, K.; Gong, B.; Peng, Q.; Parsons, G. N. Temperature-Dependent Subsurface Growth during Atomic Layer Deposition on Polypropylene and Cellulose Fibers. *Langmuir* **2010**, *26*, 8239–8244.
25. Ferguson, J. D.; Weimer, A. W.; George, S. M. Atomic Layer Deposition of Ultrathin and Conformal Al_2O_3 Films on BN Particles. *Thin Solid Films* **2000**, *371*, 95–104.
26. Ferguson, J. D.; Weimer, A. W.; George, S. M. Atomic Layer Deposition of Al_2O_3 Films on Polyethylene Particles. *Chem. Mater.* **2004**, *16*, 5602–5609.
27. Hakim, L. F.; Blackson, J.; George, S. M.; Weimer, A. W. Nanocoating Individual Silica Nanoparticles by Atomic Layer Deposition in a Fluidized Bed Reactor. *Chem. Vap. Deposition* **2005**, *11*, 420–425.
28. Although the as-assembled film in Figure 1d may appear thicker than the ALD-treated film in Figure 1e, this is due to the delamination of the former from the substrate; the two films have approximately the same thickness.
29. Yancey, S. E.; Zhong, W.; Heflin, J. R.; Ritter, A. L. The Influence of Void Space on Antireflection Coatings of Silica Nanoparticle Self-Assembled Films. *J. Appl. Phys.* **2006**, *99*, 034313(1)–034313(10).
30. Wu, Z.; Lee, D.; Rubner, M. F.; Cohen, R. E. Structural Color in Porous, Superhydrophilic, and Self-cleaning SiO_2/TiO_2 Bragg Stacks. *Small* **2007**, *3*, 1445–1451.
31. Lee, D.; Omolade, D.; Cohen, R. E.; Rubner, M. F. pH-Dependent Structure and Properties of TiO_2/SiO_2 Nanoparticle Multilayer Thin Films. *Chem. Mater.* **2007**, *19*, 1427–1433.
32. Yun, S. J.; Lee, K. H.; Skarp, J.; Kim, H. R.; Nam, K. S. Dependence of Atomic Layer-Deposited Al_2O_3 Films Characteristics on Growth Temperature and Al Precursors of $Al(CH_3)_3$ and $AlCl_3$. *J. Vac. Sci. Technol., A* **1997**, *15*, 2993–2997.
33. Shih, K. K.; Dove, D. B. Deposition of Aluminun-Oxide Films with High Refractive-Index. *J. Vac. Sci. Technol., A* **1994**, *12*, 321–322.

34. Kadali, S. B.; Soultanidis, N.; Wong, M. S. Assembling Colloidal Silica into Porous Hollow Microspheres. *Top. Catal.* **2008**, *49*, 251–258.
35. Demir-Cakan, R.; Hu, Y. S.; Antonietti, M.; Maier, J.; Titirici, M. M. Facile One-Pot Synthesis of Mesoporous SnO_2 Microspheres via Nanoparticles Assembly and Lithium Storage Properties. *Chem. Mater.* **2008**, *20*, 1227–1229.
36. Gilbert, B.; Ono, R. K.; Ching, K. A.; Kim, C. S. The Effects of Nanoparticle Aggregation Processes on Aggregate Structure and Metal Uptake. *J. Colloid Interface Sci.* **2009**, *339*, 285–295.
37. Vasiliev, P. O.; Faure, B.; Ng, J. B. S.; Bergstrom, L. Colloidal Aspects Relating to Direct Incorporation of TiO_2 Nanoparticles into Mesoporous Spheres by an Aerosol-Assisted Process. *J. Colloid Interface Sci.* **2008**, *319*, 144–151.
38. Fujii, T.; Yano, T.; Nakamura, K.; Miyawaki, O. The Sol-Gel Preparation and Characterization of Nanoporous Silica Membrane with Controlled Pore Size. *J. Membr. Sci.* **2001**, *187*, 171–180.
39. Adomaitis, R. A. Development of a Multiscale Model for an Atomic Layer Deposition Process. *J. Cryst. Growth* **2010**, *312*, 1449–1452.
40. Albo, S. E.; Broadbelt, L. J.; Snurr, R. Q. Multiscale Modeling of Transport and Residence Times in Nanostructured Membranes. *AIChE J.* **2006**, *52*, 3679–3687.
41. Lee, H. Y.; An, C. J.; Piao, S. A. J.; Ahn, D. Y.; Kim, M. T.; Min, Y. S. Shrinking Core Model for Knudsen Diffusion-Limited Atomic Layer Deposition on a Nanoporous Monolith with an Ultrahigh Aspect Ratio. *J. Phys. Chem. C* **2010**, *114*, 18601–18606.
42. Karuturi, S. K.; Liu, L. J.; Su, L. T.; Zhao, Y.; Fan, H. J.; Ge, X. C.; He, S. L.; Yoong, A. T. I. Kinetics of Stop-Flow Atomic Layer Deposition for High Aspect Ratio Template Filling through Photonic Band Gap Measurements. *J. Phys. Chem. C* **2010**, *114*, 14843–14848.
43. Cebeci, F. C.; Wu, Z. Z.; Zhai, L.; Cohen, R. E.; Rubner, M. F. Nanoporosity-driven Superhydrophilicity: A Means to Create Multifunctional Antifogging Coatings. *Langmuir* **2006**, *22*, 2856–2862.
44. Pure ALD Al_2O_3 coating has a contact angle of $55 \pm 5°$ (ref 39).
45. Kemell, M.; Farm, E.; Ritala, M.; Leskela, M. Surface Modification of Thermoplastics by Atomic Layer Deposition of Al_2O_3 and TiO_2 Thin Films. *Eur. Polym. J.* **2008**, *44*, 3564–3570.
46. Groner, M. D.; George, S. M.; McLean, R. S.; Carcia, P. F. Gas Diffusion Barriers on Polymers using Al_2O_3 Atomic Layer Deposition. *Appl. Phys. Lett.* **2006**, *88*, 051907(1)–051907(3).
47. Wilson, C. A.; Grubbs, R. K.; George, S. M. Nucleation and Growth during Al_2O_3 Atomic Layer Deposition on Polymers. *Chem. Mater.* **2005**, *17*, 5625–5634.
48. O'Hayre, R.; Feng, G.; Nix, W. D.; Prinz, F. B. Quantitative Impedance Measurement using Atomic Force Microscopy. *J. Appl. Phys.* **2004**, *96*, 3540–3549.
49. Saha, R.; Nix, W. D. Effects of the Substrate on the Determination of Thin Film Mechanical Properties by Nanoindentation. *Acta Mater.* **2002**, *50*, 23–38.
50. Tsui, T. Y.; Pharr, G. M. Substrate Effects on Nanoindentation Mechanical Property Measurement of Soft Films on Hard Substrates. *J. Mater. Res.* **1999**, *14*, 292–301.
51. Hay, J.; Crawford, B. Measuring Substrate-Independent Modulus of Thin Films. *J. Mater. Res.* **2011**, *26*, 727–738.
52. Walter, C.; Mitterer, C. 3D versus 2D Finite Element Simulation of the Effect of Surface Roughness on Nanoindentation of Hard Coatings. *Surf. Coat. Technol.* **2009**, *203*, 3286–3290.
53. Schulz, U.; Lau, K.; Kaiser, N. Antireflection Coating with UV-protective Properties for Polycarbonate. *Appl. Opt.* **2008**, *47*, C83–C87.
54. Minton, T. K.; Wu, B. H.; Zhang, J. M.; Lindholm, N. F.; Abdulagatov, A. I.; O'Patchen, J.; George, S. M.; Groner, M. D. Protecting Polymers in Space with Atomic Layer Deposition Coatings. *ACS Appl. Mater. Interfaces* **2010**, *2*, 2515–2520.
55. Triani, G.; Campbell, J. A.; Evans, P. J.; Davis, J.; Latella, B. A.; Burford, R. P. Low Temperature Atomic Layer Deposition of Titania Thin Films. *Thin Solid Films* **2010**, *518*, 3182–3189.
56. Chunder, A.; Etcheverry, K.; Wadsworth, S.; Boreman, G. D.; Zhai, L. Fabrication of Anti-Reflection Coatings on Plastics using the Spraying Layer-by-Layer Self-Assembly Technique. *J. Soc. Inf. Disp.* **2009**, *17*, 389–395.
57. Elam, J. W.; Xiong, G.; Han, C. Y.; Wang, H. H.; Birrell, J. P.; Welp, U.; Hryn, J. N.; Pellin, M. J.; Baumann, T. F.; Poco, J. F.; *et al.* Atomic Layer Deposition for the Conformal Coating of Nanoporous Materials. *J. Nanomater.* **2006**, *2006*, 1–5.
58. Elam, J. W.; Libera, J. A.; Pellin, M. J.; Zinovev, A. V.; Greene, J. P.; Nolen, J. A. Atomic Layer Deposition of W on Nanoporous Carbon Aerogels. *Appl. Phys. Lett.* **2006**, *89*, 053124(1)–053124(3).
59. Gusev, E. P.; Copel, M.; Cartier, E.; Baumvol, I. J. R.; Krug, C.; Gribelyuk, M. A. High-Resolution Depth Profiling in Ultrathin Al_2O_3 Films on Si. *Appl. Phys. Lett.* **2000**, *76*, 176–178.
60. Hausmann, D. M.; de Rouffignac, P.; Smith, A.; Gordon, R.; Monsma, D. Highly Conformal Atomic Layer Deposition of Tantalum Oxide using Alkylamide Precursors. *Thin Solid Films* **2003**, *443*, 1–4.
61. Knez, M.; Niesch, K.; Niinisto, L. Synthesis and Surface Engineering of Complex Nanostructures by Atomic Layer Deposition. *Adv. Mater.* **2007**, *19*, 3425–3438.
62. TiO_2/SiO_2 nanoparticle LbL films treated at 150 °C for 10 min without the ALD reactions have poor mechanical durability. When such films are gently abraded with Kimwipes, the films are easily removed from their substrates (*e.g.*, glass slides). This result indicates that 150 °C thermal treatment alone does not impart mechanical robustness to TiO_2/SiO_2 LbL films.
63. Mori, S.; Okamoto, H. A Unified Theory of Determining the Electrophoretic Velocity of Mineral Particles in the Rectangular Micro-Electrophoresis Cell. *J. Flotation Res. Assoc. Jpn.* **1980**, *27*, 117–126.